Genesis of Tropical Storm Eugene (2005) from Merging Vortices Associated with ITCZ Breakdowns. Part I: Observational and Modeling Analyses

CHANH Q. KIEU AND DA-LIN ZHANG

Department of Atmospheric and Oceanic Science, University of Maryland, College Park, Maryland

(Manuscript received 29 August 2007, in final form 8 May 2008)

ABSTRACT

Although tropical cyclogenesis occurs over all tropical warm ocean basins, the eastern Pacific appears to have the highest frequency of tropical cyclogenesis events per unit area. In this study, tropical cyclogenesis from merging mesoscale convective vortices (MCVs) associated with breakdowns of the intertropical convergence zone (ITCZ) is examined. This is achieved through a case study of the processes leading to the genesis of Tropical Storm Eugene (2005) over the eastern Pacific using the National Centers for Environmental Prediction reanalysis, satellite data, and 4-day multinested cloud-resolving simulations with the Weather Research and Forecast (WRF) model at the finest grid size of 1.33 km.

Observational analyses reveal the initiations of two MCVs on the eastern ends of the ITCZ breakdowns that occurred more than 2 days and 1000 km apart. The WRF model reproduces their different movements, intensity and size changes, and vortex–vortex interaction at nearly the right timing and location at 39 h into the integration as well as the subsequent track and intensity of the merger in association with the poleward rollup of the ITCZ. Model results show that the two MCVs are merged in a coalescence and capture mode due to their different larger-scale steering flows and sizes. As the two MCVs are being merged, the low- to midlevel potential vorticity and tangential flows increase substantially; the latter occurs more rapidly in the lower troposphere, helping initiate the wind-induced surface heat exchange process leading to the genesis of Eugene with a diameter of 400 km. Subsequently, the merger moves poleward with characters of both MCVs. The simulated tropical storm exhibits many features that are similar to a hurricane, including the warm-cored "eye" and the rotating "eyewall." It is also shown that vertical shear associated with a midlevel easterly jet leads to the downshear tilt and the wavenumber-1 rainfall structures during the genesis stage, and the upshear generation of moist downdrafts in the vicinity of the eyewall in the minimum equivalent potential temperature layer. Based on the above results, it is concluded that the ITCZ provides a favorable environment with dynamical instability, high humidity, and background vorticity, but it is the merger of the two MCVs that is critical for the genesis of Eugene. The storm decays as it moves northwestward into an environment with increasing vertical shear, dry intrusion, and colder sea surface temperatures. The results appear to have important implications for the high frequency of development of tropical cyclones in the eastern Pacific.

1. Introduction

The life cycle of tropical cyclones (TCs) is typically divided into the following four phases: pregenesis with little closed circulation, tropical depression (TD), tropical storm (TS), and hurricane. Of the four, the pregenesis and its subsequent growth to TD and TS stages, the so-called tropical cyclogenesis (TCG), are the most difficult phases to predict by numerical TC models and operational forecasters. Despite the many processes involved during TCG, the recent successes of global models in predicting TC tracks indicate that the large-scale circulation is the key parameter in determining where TCG may occur. It is well known that the large-scale conditions conducive for TCG over different ocean basins include weak vertical wind shear (Gray 1968; McBride and Zehr 1981; DeMaria 1996), warm sea surface temperature (SST) and deep moist layers (Emanuel 2000), well-organized angular momentum fluxes (Challa and Pfeffer 1990), easterly waves (Molinari et al. 2000), active Madden–Julian oscillations, and unstable background flows (Molinari et al. 1997). Some large-scale influences on TCG—such as monsoon

Corresponding author address: Dr. Da-Lin Zhang, Department of Atmospheric and Oceanic Science, University of Maryland, College Park, MD 20742–2425.
E-mail: dalin@atmos.umd.edu

DOI: 10.1175/2008JAS2605.1

troughs, upper-level troughs, cold surges, elevated dust layers, and topographical effects—may be more relevant over one ocean basin than the others.

Although TCG may be mostly dictated by large-scale dynamics, recent observational and modeling studies show growing evidence of the important roles of mesoscale convective vortices (MCVs) in promoting TCG. For example, Bosart and Sanders (1981), Harr and Elsberry (1996), Harr et al. (1996), and Zhang and Bao (1996a,b) showed TCG as induced by single well-defined MCVs associated with mesoscale convective systems (MCSs). Using satellite and research aircraft data, Ritchie and Holland (1997, hereafter RH97) studied the interaction of midlevel MCVs with a low-level large-scale trough in the formation of Typhoon Irving (1992). They found that the initial interaction of the low-level trough and a midlevel cyclonic circulation associated with an upper-level trough resulted in the formation of TD Irving. The subsequent merger of the MCVs, which were embedded within the background TD vortex, contributed midlevel vorticity to the amplification of the storm and led to rapid transitioning to TS stage. Similarly, Simpson et al. (1997) examined the rotating and merging interaction of two MCVs with a monsoon trough in the genesis of TS Oliver (1993). They noted that the MCVs could initiate new MCSs, following a period of little convective activity, and then they merged into the monsoon low with one becoming the eye and the other forming a spiral rainband of the storm. In both cases, the large-scale cyclonic flows appear to set up favorable environments, but it is the mesoscale processes that determine the timing and location of TCG. Reasor et al. (2005) documented the existence of even smaller-scale (mesoγ) vortices from radar observations during the early development of Hurricane Dolly (1996). However, the transitioning from a pre-Dolly disturbance to a hurricane occurred rapidly so that the genesis phase of Dolly was not easy to define. As in RH97, the merger of multiple MCVs took place within a larger-scale cyclonical flow.

While TCG can occur over all tropical warm ocean basins, the eastern Pacific appears to experience the highest density of TCG events (Gray 1968). In the view of operational forecasters, many eastern Pacific TCs can be traced back to African easterly waves that propagate across the Atlantic and Central America and then into the eastern Pacific (Avila and Pasch 1992). Numerous studies showed that the eastern Pacific TCG could occur in association with MCSs (Bister and Emanuel 1997), easterly waves in the intertropical convergence zone (Molinari et al. 2000; Dickinson and Molinari 2002), and the interaction of easterly waves with the Central American mountains (Zehnder et al. 1999). Satellite observations revealed that the ITCZ may sometimes undulate and break down into a series of mesoscale disturbances or MCVs, some of which may grow into TCs (Agee 1972; Hack et al. 1989; Wang and Magnusdottir 2006, hereafter WM06). Theoretical studies indicated that the ITCZ breakdown and its subsequent poleward rollup are closely related to the Charney–Stern (i.e., combined barotropic and baroclinic) instability, and could also be triggered by propagating easterly disturbances (Nieto Ferreira and Schubert 1997, hereafter NS97; WM06). Because of the frequent ITCZ breakdowns during the warm season, this mechanism has been suggested to explain why the eastern Pacific tends to be more active in TCG (see NS97; WM06).

Despite many important findings in the previous studies, few have examined multiscale processes involved in TCG over the eastern Pacific and other ocean basins. In particular, the exact nature of interactions among the ITCZ, easterly disturbances or MCVs, vertical wind shear (VWS), cloud clusters, orography, and TCG still remains elusive because of the lack of high-resolution, quality data over tropical oceans. For this reason, the National Aeronautics and Space Administration conducted the Tropical Cloud System Processes (TCSP) field campaign in July 2005 using various state-of-the-art observing systems, including aircraft measurements and satellite observations (Halverson et al. 2007).

The purposes of the present study are to (i) document the full life cycle of a TS from its pregenesis to dissipation stages over a period of 11 days; (ii) investigate TCG from merging MCVs associated with the ITCZ breakdowns/rollup; and (iii) examine the impact of VWS and other processes on the structural changes in precipitation and vertical motion during the genesis and subsequent dissipation of the storm. This will be achieved by using the National Centers for Environmental Prediction (NCEP) $1^\circ \times 1^\circ$ reanalysis and satellite data and performing 4-day (i.e., 0000 UTC 17–21 July 2005) cloud-resolving simulations of the life cycle of TS Eugene (2005) during the TCSP field campaign using the Weather and Research Forecast (WRF) model [Advanced Research WRF (ARW), V2.1.2] with the finest grid size of 1.33 km.

The next section provides a large-scale overview of TS Eugene (2005) from its origin to dissipation using the NCEP reanalysis and satellite data. Section 3 describes all necessary parameters used in the WRF model for the control simulation. Section 4 shows model verification against available observations. Some simulated nonobservable features and sensitivity simulations will also be discussed. Section 5 presents the

three-dimensional structures and evolution and the merger of two propagating MCVs in relation to the genesis of Eugene. Section 6 examines the dynamical and thermodynamic effects of VWS as well as the other environmental conditions on the development of the storm. A summary and conclusions are given in the final section.

2. Overview

According to the official report of the National Weather Service and the National Hurricane Center, TS Eugene (2005) had its origin from a traveling tropical wave entering the Caribbean Sea on 10 July 2005. However, multiple MCVs and vigorous convective activities within the ITCZ make the report questionable. The Hovmöller diagram of the 850-hPa relative vorticity field (Fig. 1a), satellite imageries (Fig. 2), and the model simulation (to be presented in section 4) show that Eugene (denoted by the letter "E" after it was upgraded to a TD) was actually growing out of two merged MCVs: a southeasterly disturbance or MCV initiated before 0000 UTC 11 July on the eastern end of the ITCZ offshore of Costa Rica (near 8°N, 84°E; see Figs. 1b,c) and an MCV spawned from the ITCZ on 13 July 1000 km to the west (hereafter referred to as V_1 and V_2, respectively; Fig. 1a). The associated TS watch, which appeared to be based just on the evolution of V_1, was first issued at 1500 UTC 18 July for a location ~200 km to the south of Manzanillo, Mexico. Speculating on the possibility of the formation of a TC within this active area, the TCSP team conducted several experiments with the NASA ER-2 and NOAA P-3 mission aircraft during the pregenesis stage (15–16 July). Even though at many instances the aircraft captured several midlevel MCVs and deep convective towers in the ITCZ, the area covered by the aircraft (5°–11°N, 91°–85°W) was nonetheless southeast of the actual region where Eugene developed (9°–14°N, 104°–99°W). In addition, the precursor for Eugene was not well defined at this flight time (see Halverson et al. 2007 and Fig. 1 herein).

Although V_1 could be traced back up to 7 days before Eugene's depression stage (Fig. 1), NCEP's $1° \times 1°$ resolution reanalysis does not indicate any connection of V_1 to any propagating easterly wave with typical wavelength of 2000–3000 km from 0000 UTC 11 July to 0000 UTC 16 July 2005. Instead, several MCVs entered the Caribbean Sea during this period but did not survive after propagating across the Central American cordillera. Both satellite observations and the NCEP reanalysis show that V_1 appeared to be related to one of the ITCZ breakdown episodes at 0000 UTC 11 July

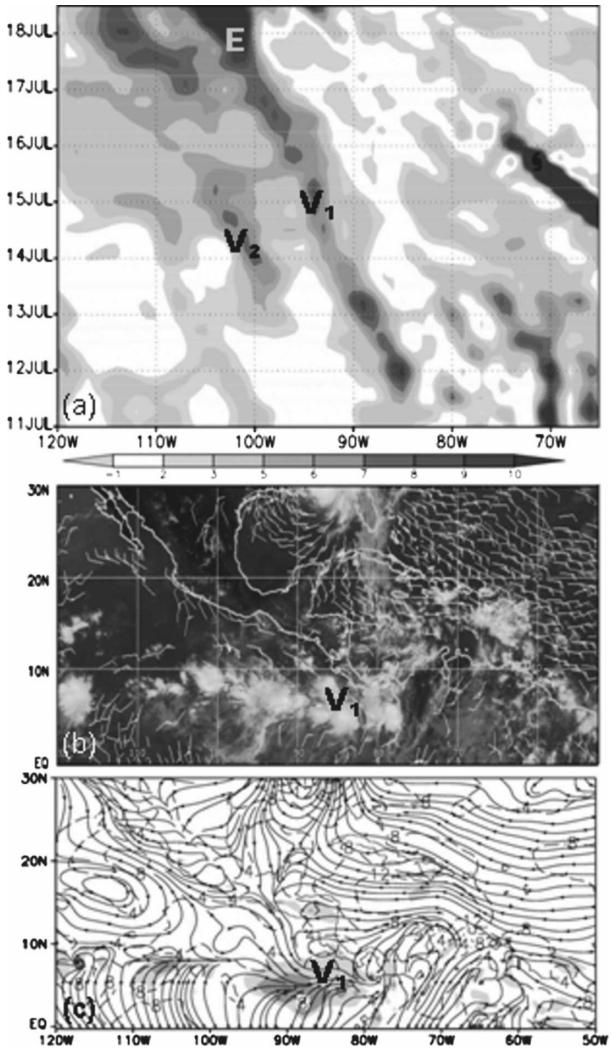

FIG. 1. (a) Hovmöller diagram of the vertical absolute vorticity (10^{-5} s^{-1}) at 850 hPa during the period from 0000 UTC 11 to 1200 UTC 18 Jul 2005 and the longitudinal span of 120°–65°W that is obtained by meridionally averaging three slices (i.e., 3°) of the NCEP reanalysis following the V_1 center, starting at 8°N. (b) Geostationary Operational Environmental Satellite, *GOES-10/12* images of clouds, superimposed by the low-level winds valid at 0000 UTC 11 Jul 2005. (c) NCEP reanalysis of the 850-hPa streamlines (solid), isotachs (dashed, every 2 m s^{-1}), and relative humidity (shaded for 85% and 95%). The two MCVs associated with the formation of TS Eugene (shown as "E") are denoted V_1 and V_2; similar conventions are used for the rest of the figures. Hurricane symbol marks the evolution of Emily (2005). Note that V_2 does not exist before 0000 UTC 13 Jul.

(Figs. 1b,c); however, it could not be traced farther back due partly to its relatively small scale and partly to its weak intensity. One may note from Fig. 1a, plotted from the 6-hourly NCEP reanalysis, that Eugene looks as if it grew out of V_1. However, the 3-hourly satellite imageries show that the V_1-related cloud system, exhib-

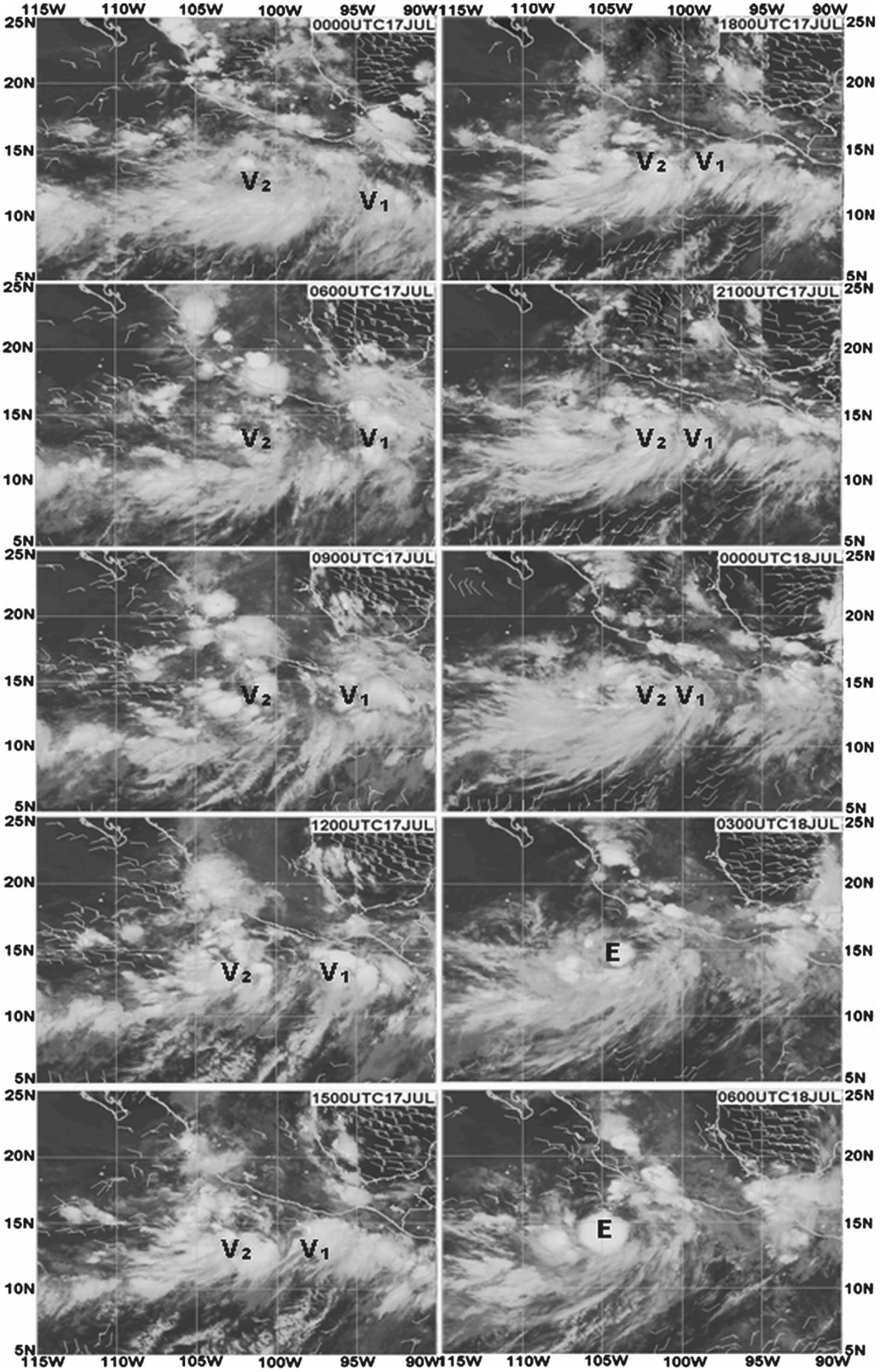

FIG. 2. *GOES-10/12 CIMSS* images of clouds, superimposed by the low-level winds, from 0000 UTC 17 to 0000 UTC 21 Jul 2005. More frequent time frames are shown during the period from 0600 UTC 17 to 0900 UTC 18 Jul to show better the merger of V_1 and V_2.

iting rotational "solid" cloud signatures during the period of 0600–1500 UTC 17 July, shrank in size although it kept intensifying (under the constraint of angular momentum conservation) as it moved at a mean speed of about 3.3 m s^{-1} offshore along the Mexican coast under the influence of southeasterly flows plus the earth curvature (β) effect (see Li and Wang 1994). In contrast, V_2 moved at a speed similar to V_1 during the first 3 days after its formation, but it was quasi stationary zonally after 0000 UTC 16 July (Fig. 1). Instead, V_2 began to move slowly northward as the rollup of the ITCZ. The V_2-related cloud system exhibited better mesoscale organization and more distinct rotation than V_1 at 0000 UTC 17 July and then expanded in size but likely weakened during its northward displacement. Both V_1 and V_2 possessed comparable size and organization at 0600 UTC 17 July. It appears to be their subsequent merger (i.e., from 2100 UTC 17 to 0600 UTC 18 July), to be shown in sections 4 and 5, that caused the emergence of TD Eugene.

Although the NCEP reanalysis may be too coarse to resolve properly the MCVs, especially V_1 at the later stages, we use Fig. 3 to show two distinct upright vortical columns corresponding to V_1 and V_2 a few hours prior to the merger, and a single deeper and more robust vortex merger (E) afterward, in contrast to the other MCSs in the ITCZ, which exhibit little, or weak, vortical signature (cf. Figs. 1–3). The two MCVs have comparable magnitudes in relative vorticity and depth, but V_2 displays a larger-scale rotation, consistent with those seen from satellite imagery (cf. Figs. 2 and 3a). However, the NCEP reanalysis does not show evidence of closed cyclonic circulations at the surface associated with V_1 and V_2 at 0000 UTC 17 July—to be used as the model initial time—except for an elongated low pressure region along the ITCZ (Fig. 4a).

Figures 4 and 5 show the large-scale conditions in which the genesis of Eugene occurred. The most distinct large-scale feature is the east–west oriented ITCZ over the tropical eastern Pacific and its associated converging flows between the southeasterly and the northeasterly trade winds from the Southern and Northern Hemisphere, respectively. However, the trade winds (and the ITCZ) were no longer pronounced, at least in the boundary layer, over the land masses of southern Mexico and Central America. In particular, the complex topography and its associated temperature contrast across the coastline over the area between the equator and 15°N distorted the trade wind pattern and generated a weak pressure trough offshore (Fig. 4a). Because of the topographical effect, the southeasterly trade winds were shifted more to southwesterly, that is, landward to the south of the ITCZ.

Note that the lower sea level pressure centers over continental Mexicot are fictitious because they result from the pressure reduction associated with high orography and high surface temperatures in the NCEP reanalysis. Nevertheless, the lee side of the high orography over the area appeared to be a favorable region for TCG in the eastern Pacific, as discussed by Zehnder

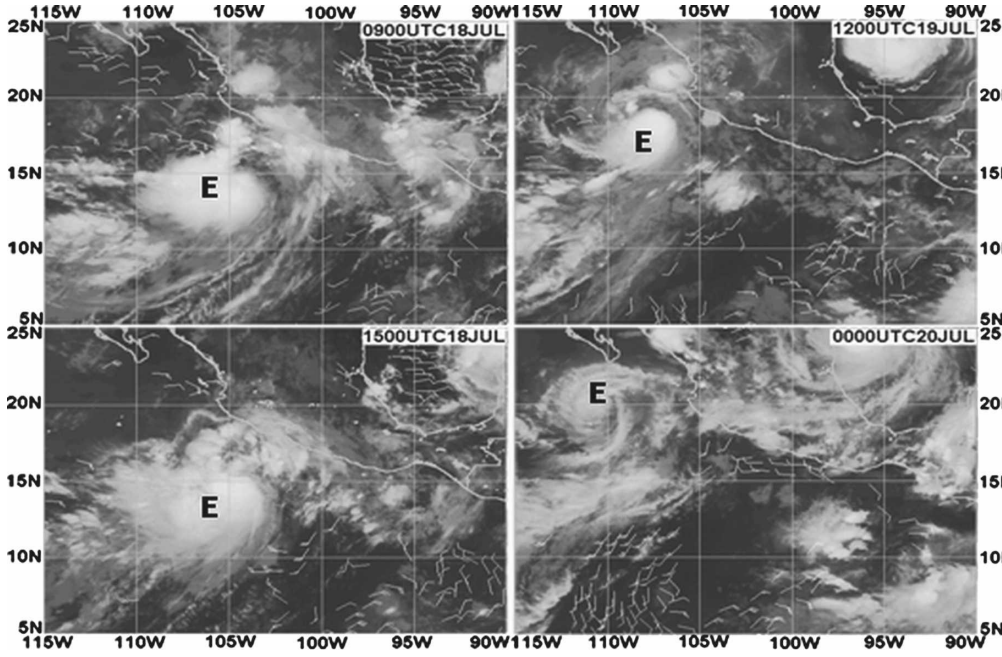

FIG. 2. (*Continued*)

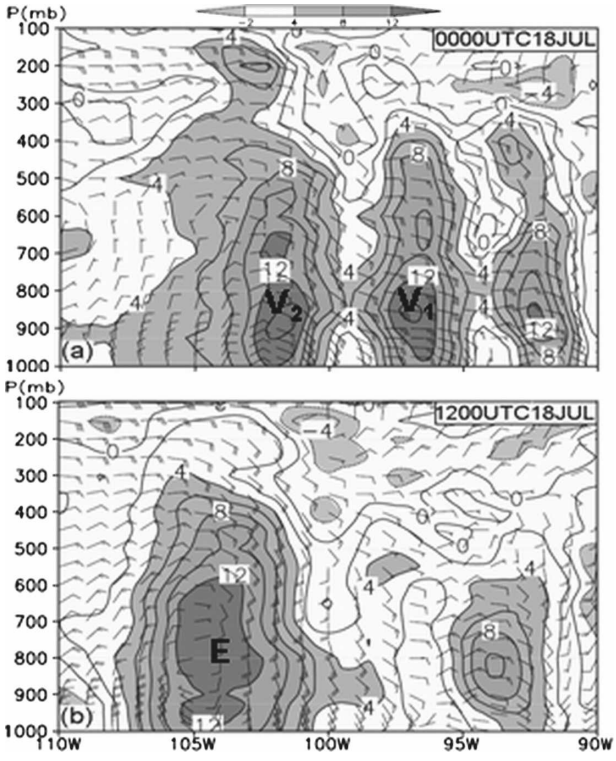

FIG. 3. West–east vertical cross sections from the NCEP reanalysis of the vertical absolute vorticity area averaged within a 3° latitudinal span centered along 14°N, at intervals of 2×10^{-5} s^{-1}, superimposed by in-plane horizontal wind barbs, along the two vortex centers, valid at (a) 0000 UTC and (b) 1200 UTC 18 Jul 2005. Absolute vorticity values greater than 4, 8, and 12 ($\times 10^{-5}$ s^{-1}) are shaded.

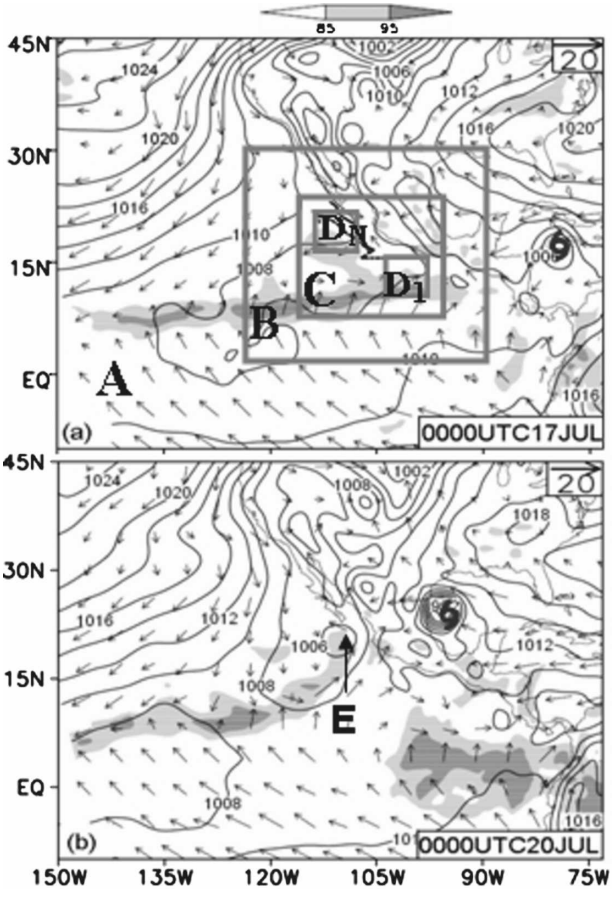

FIG. 4. NCEP reanalysis of sea level pressure (solid, every 2 hPa), horizontal flow vectors, and relative humidity (shaded for 85% and 95%) at 900 hPa for 0000 UTC (a) 17 Jul and (b) 20 Jul 2005. The model meshes with horizontal resolutions of 36, 12, 4, and 1.33 km for domains A, B, C, and D are, respectively, sketched in (a), along with the observed (thick solid) and simulated (thick dashed) tracks. The finest domain D follows the movement of the storm, and D_1 and D_N denote the first and the last position of domain D.

et al. (1999) and Molinari et al. (2000). Note also that the low pressure system moving over the Gulf of Mexico is Hurricane Emily (2005), a category-4 storm that occurred during TCSP (see Halverson et al. 2007). The other large-scale features include an intense anticyclonic circulation in the eastern Pacific and an anticyclonic ridge extending westward along the southern coast of the United States.

In a vertical plane, the trade wind convergence zone is characterized by southwesterly flow turning clockwise with height and southeasterly flow turning anticlockwise to easterlies above 850 hPa to the south and north of the ITCZ, respectively (Figs. 4 and 5a). Note the development of a midlevel jet of 10–12 m s^{-1} on each side, that is, along 17° and 10°N. The two jets are qualitatively supported by the thermal wind relation, as indicated by significant temperature gradients on both sides of the ITCZ (Fig. 5c). Such pronounced easterly and westerly flows imply the presence of significant cyclonic shear, that is, an averaged shear vorticity of 3×10^{-5} s^{-1} in the ITCZ, which was the important background vorticity for the genesis of Eugene. More importantly, they account for changes in the sign of potential vorticity (PV) gradients near the inflection point of the zonal flows (Fig. 5b), suggesting that the basic state in the vicinity of the ITCZ was both barotropically and baroclinically unstable (Charney and Stern 1962). NS97 show that the Charney–Stern instability is a necessary condition for the ITCZ breakdown and rollup as a result of the development of MCVs, whereas Molinari et al. (1997, 2000) indicate that the sign reversal of PV gradients is one of the important signals for TCG. Since diabatic heating in the ITCZ tends to generate a low-level PV maximum and a sign reversal in the meridional PV gradient (see NS97), the ITCZ is generally a favorable region for the develop-

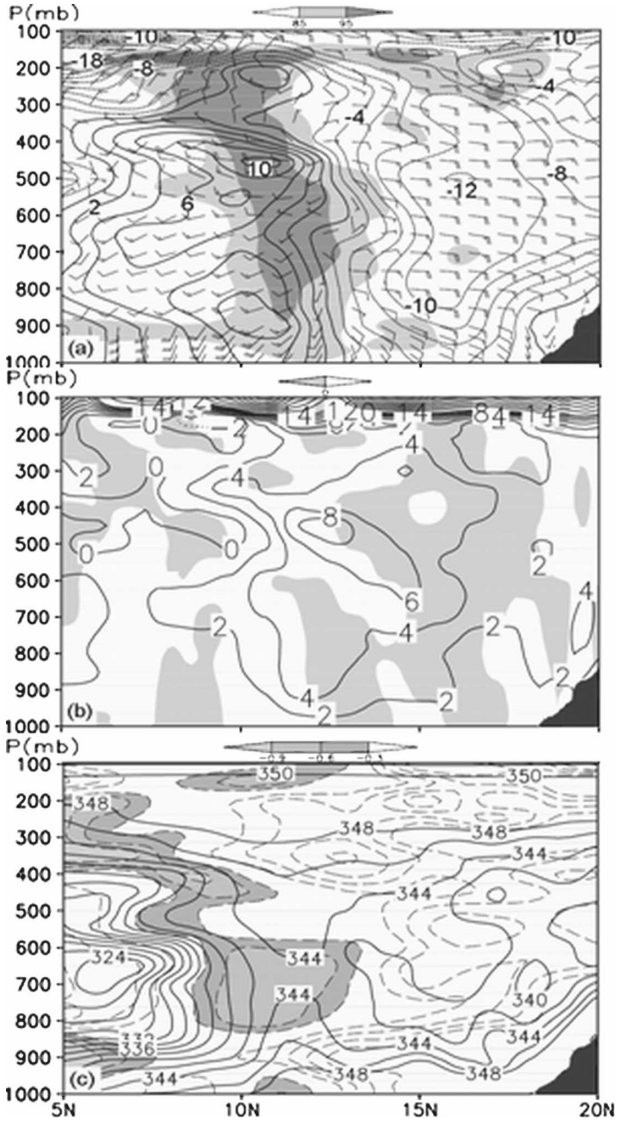

FIG. 5. North–south vertical cross sections along 103°W from the NCEP reanalysis at 0000 UTC 17 Jul 2005 of (a) zonal wind speeds (at intervals of 2 m s^{-1}), superimposed with horizontal wind barbs (a full barb is 5 m s^{-1}), and relative humidity (shaded for >85% and >95%); (b) PV (at intervals of 0.2 PVU; 1 PVU = 10^{-6} m^2 s^{-1}K kg^{-1}) and meridional PV gradient (shaded for negative values); and (c) equivalent potential temperature θ_e (solid, at intervals of 2 K), superimposed by deviation temperature (dashed, at intervals of 0.3 K, shaded for negative values). Shading at the lower right corner denotes terrain over Mexico.

ment of mesovortices or TCG. In the present case, the zone of such a sign reversal was virtually upright and collocated with a weak-sheared ITCZ environment in which the precursor of Eugene (i.e., V_2) was embedded (cf. Figs. 4a and 5a,b). Evidently, this ITCZ breakdown resulted from the growth of V_2, which differs from that associated with the development of V_1 more than 2 days earlier (i.e., before 11 July) and 1000 km to the southeast at 0000 UTC 13 July: V_1 and V_2 were 750 km apart along the ITCZ at the model initial time (see Fig. 1).

Figures 5a and 5c also show that the ITCZ was characterized by high humidity with a relatively cold pool below and warm air above as a result of continued deep convective overturning. The atmospheric conditions outward from the ITCZ are potentially unstable, with higher low-level equivalent potential temperature θ_e to the north where high SST was distributed (Fig. 5c). These thermodynamic conditions are similar to the idealized initial conditions used by Bister and Emanuel (1997) in their axisymmetric modeling of a hurricane, in which a cold-core midlevel mesovortex with humid columns can be spun up into a hurricane within 3 days. They emphasized the critical roles of the initial vortex intensity and humid environment in the genesis of Hurricane Guillermo (1991). In the present case, Eugene appeared to be initiated from the merger of the two MCVs that were embedded in the moist ITCZ. Evidently, the high moisture content in the ITCZ is also the major energy source for intensification of the storm.

Since Eugene moved northwestward after its formation, it is also of interest to examine the relation of Eugene's development to the midlevel easterly jet. The NCEP reanalysis reveals that this jet, occurring within the latitude belt 15°–20°N, was a persistent feature; it appeared nearly 10 days prior to Eugene's formation. The jet-related VWS appears to limit the growth of Eugene after reaching its peak intensity at 1200 UTC 19 July, with minimum sea level pressure 989 hPa and maximum surface wind 31 m s^{-1} (Figs. 2 and 7). In addition, colder SST, separation from the ITCZ, dry intrusion, and some other factors to be discussed in section 6 all played important roles in weakening the storm. By late in the day of 20 July, Eugene became a remnant low about 100 km southwest of Cabo San Lucas (see Fig. 2). It continued its northwestward movement until its dissipation 2 days later.

3. Model description

In this study, the processes leading to the genesis of TS Eugene (2005) are explicitly simulated using a two-way interactive, movable, multinested (36/12/4/1.33 km) grid version of the nonhydrostatic Weather Research and Forecast model (V2.1.2) (see Skamarock et al. 2005) with the finest grid size of 1.33 km. The model microphysics schemes used include (i) a modified version of the Kain and Fritsch (1990) cumulus parameter-

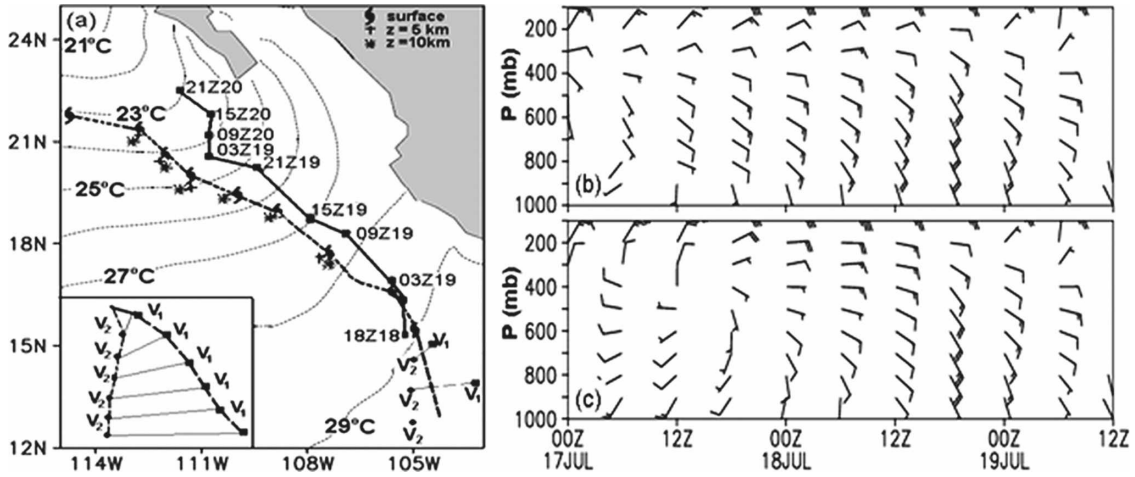

FIG. 6. (a) Comparison of the simulated track (dashed) of Eugene to the best-track analysis (solid), superimposed by the SST field (dotted) at intervals of 1°C. The simulated minimum pressure positions of Eugene at the three selected model levels (z = 0, 5, 10 km) are also shown. Note that the model-data points are given at the corresponding best-track analysis times. The lower left corner enlarges the tracks of both V_1 and V_2, based on their 850-hPa relative vorticity and surface pressure centers, from 18 Jul 0000 UTC 24 hours into the integration (or 18/00–24) to 18/18–39 at 3-h intervals. (b), (c) Time–height cross section of the (400 km × 400 km) area-averaged horizontal wind barbs centered at (b) V_1 and (c) V_2 from 17/00–00 to 19/12–60. Note that the wind barbs in (b) and (c) become more similar after 18/06–30 and identical after 18/18–39 owing to their merging.

ization scheme for the 36- and 12-km resolution domains in which deep convection and a broad range of shallow convection are both parameterized; (ii) the Yonsei University planetary boundary layer (PBL) parameterization with the Monin–Obukhov surface layer scheme; (iii) the Rapid Radiative Transfer Model (RRTM) scheme for both longwave and shortwave radiation (Mlawer et al. 1997); and (iv) the Lin et al. (1983) cloud microphysics scheme containing six classes of hydrometeors, namely, water vapor, cloud water, rain, snow, graupel, and cloud ice. Note that no cumulus parameterization is used in the 4- and 1.33-km resolution domains.

The four nested grid domains have the (x, y) dimensions of 251 × 201 (A), 252 × 252 (B), 388 × 382 (C), and 451 × 451 (D) with a grid size of 36, 12, 4, and 1.33 km, respectively (see Fig. 4a for the nested domains A–D). There are 38 σ levels in the vertical: 1.000, 0.993, 0.980, 0.966, 0.950, 0.933, 0.913, 0.892, 0.869, 0.844, 0.816, 0.786, 0.753, 0.718, 0.680, 0.643, 0.607, 0.572, 0.538, 0.505, 0.473, 0.441, 0.409, 0.378, 0.348, 0.318, 0.289, 0.260, 0.232, 0.204, 0.176, 0.149, 0.122, 0.095, 0.068, 0.042, 0.018, and 0.000. The model top is defined at 30 hPa. To minimize computational costs, domain D is activated at 24 h into the integration and it is moved within domain C every 15 min following the storm. In this control simulation, the domain D movement is performed manually because the storm's pressure center is too weak to be determined by the model prior to the merger of the two MCVs. Because of limited computer power, domain D is configured to cover only the area where V_1 and V_2 are about 500 km apart rather than where they are initially present.

The WRF model is initialized at 0000 UTC 17 July 2005, about 39 h before the best track began, and then integrated for 4 days until the storm is nearly dissipated. No bogus data is used. Despite its 1° resolution, the NCEP reanalysis appears to resolve marginally the two MCVs under study with diameters of ~400 km at the model initial time, as compared to those seen in satellite imaginary. Nonetheless, a successful simulation of the case will allow us to examine the genesis of a TC from weak midlevel MCVs to a TS and its subsequent dissipation in the eastern Pacific environment, which could not be studied with the NCEP reanalysis data.

The model initial and lateral boundary conditions are taken from the NCEP reanalysis with the outermost lateral boundaries updated every 6 h. The NCEP SST field is used and kept constant in time (Fig. 6); its magnitude decreases from 29° to 23°C northwestward along Eugene's track. This choice of keeping SST constant is justified by negligible temporal variation of the SST during the model integration period, based on the analysis of the Tropical Rainfall Measuring Mission (TRMM) Microwave Imager (TMI) level-1 product (not shown). In addition, there is little evidence of storm-induced cooling along its track owing to the generation of relatively weaker surface winds by the storm.

4. Model verification

In this section, we validate the model-simulated results against the best-track analysis and satellite observations since few field observations were available for this storm (Halverson et al. 2007). We will focus more on the storm-scale cloud/precipitation in relation to the evolution of the MCVs, their merger, and the ITCZ. Due to the small domain size of the 1.33-km grid, some results will be presented from the 4-km grid to show better the storm–environment interaction.

Figure 6a compares the simulated track of Eugene, based on the minimum sea level pressure, to the best-track analysis. It is evident that the WRF model reproduces reasonably well the track of Eugene, especially the timing and location of its genesis at 39 h into the integration. However, the simulated track tends to possess a southwestward bias at later stages, leading to an ~380 km southwestward departure from the observed at the end of the 96-h simulation. This southwestward bias appears to be related to the southwestward (downshear) tilt of the storm's circulation center with height (Fig. 6a) because a stronger storm than the observed is simulated (Fig. 7). This may be understood through the upper- and lower-level vortex–vortex interaction in the presence of VWS (see Wu and Emanuel 1993; Jones 1995). That is, the convectively generated upper-level PV anomaly tilting to the southwest of the storm under the influence of easterly VWS may induce a low pressure circulation beneath, thereby "pulling" the surface low center southwestward from its normal track. To validate this conjecture, a sensitivity experiment in which both shortwave and longwave radiation schemes are switched off from the control run is conducted in an attempt to obtain a weaker storm (not shown), based on the previous TC modeling studies (e.g., Liu et al. 1997). As expected, the model produces a weaker, shallower TC but with its track closer to the observed because of the smaller influence of the upper-level flows. This indicates that the TC intensity, if not accurately predicted, could cause large errors in its predicted track in the presence of larger-scale VWS. Note that the influence of VWS on the TC track presented in this paper differs from that in previous studies in which the leftward or rightward biases of TC movements in the presence of strong VWS are addressed (Wu and Emanuel 1993; Wang and Holland 1996). In those studies, TCs move along VWS vectors, whereas the VWS vector here is almost orthogonal to Eugene's track (cf. Figs. 6a and 12).

Figure 6a also shows the relative positions of the simulated V_1 and V_2 during an 18-h period prior to their merger. One can see from Figs. 2 and 6a that V_2 moves north-northeastward on the eastern end of the ITCZ as the latter rolls up as a result of dynamical instability, whereas V_1 moves at a faster pace northwestward under the influence of the low to midlevel southeasterly flow offshore along the Mexican coast (cf. Figs. 1, 2, and 6b,c). Thus, they appear to occur as the coalescence of two vortex entities (as described by Lander and Holland 1993) due to their different propagation speeds and directions associated with different larger-scale steering flows (cf. Figs. 6b,c)—resulting in the capture of the smaller vortex by the larger one (i.e., V_1 by V_2). Note that V_2 does not change its northward course (but does so its speed) until the two centers are less than 120 km apart at 1500 UTC 18 July, 39 h into the integration (hereafter referred to as 18/15–39), implying that V_1's radius of maximum wind (RMW) has intersected with that of V_2. These scenarios appear to differ from the TCG cases observed by RH97 and Simpson et al. (1997) in which midlevel MCVs were merged within a low-level larger-scale cyclonic circulation. This implies that the merger would sooner or later take place within the larger-scale cyclonic system. However, in the present case, only when V_1 and V_2 come

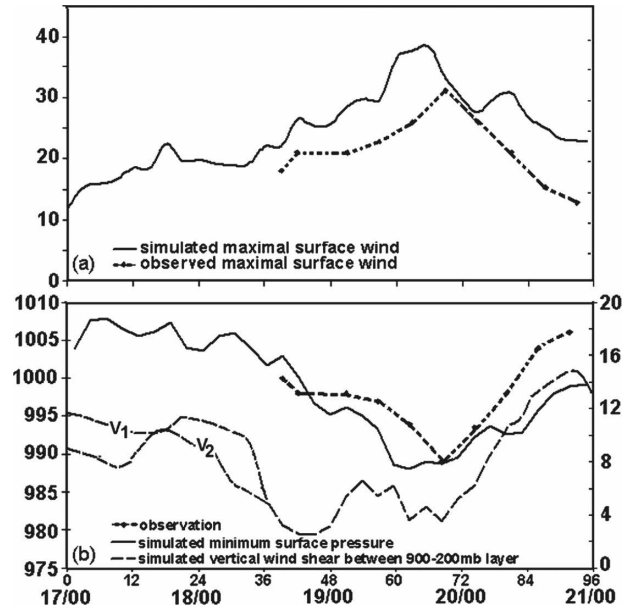

FIG. 7. Time series of (a) the simulated (solid) maximum surface wind ($m\ s^{-1}$) vs the observed (dotted) and (b) the simulated (solid) minimum sea level pressure (hPa) vs the observed (dotted) during the 4-day period from 17/00–00 to 21/00–96. Note that the best-track analysis is only available during the final 54 h. The time evolution of the area-averaged (800 km × 800 km) VWS (long dashed; $m\ s^{-1}$) in the layer of 200–900 hPa is also shown in (b). VWS during the first 36-h simulation is taken around the V_1 and V_2 centers within an area of 400 km × 400 km because of their reducing distance with time.

into near proximity (e.g., less than 450 km between their centers) does the vortex–vortex interaction tend to slow the north-northwestward movement of V_2 and accelerate slightly the northwestward displacement of V_1, both in spiral orbits, until the two MCVs completely merge. Clearly, they would not merge if there were some changes in their tracks. To our knowledge, the coalescence and capture of MCVs leading to the formation of a TD have not been reported in the literature. After the merger, both observed and simulated storms move northwestward, following closely the track and speed of V_1 but still behaving like the rollup of the ITCZ as V_2 for a while (see Figs. 2, 4b, and 6a).

The simulated minimum sea level pressure and maximum surface wind are compared to the observed in Fig. 7, which shows that the model captures the major characteristics of Eugene including its genesis, significant deepening, and intensity changes as well as its final weakening. As expected, the simulated maximum intensity is stronger than the observed—that is, about 2 hPa deeper and 8 m s^{-1} higher—because of the use of higher-resolution gridpoints; but it occurs 6 h earlier than the observed. Furthermore, the simulated storm weakens at a rate slower than observed, due partly to its farther westward tracking out to the open ocean than observed; this would cause access of relatively less continental dry air masses (but more oceanic moist air) to suppress the storm development.

Of interest is that the (area-averaged) environmental VWS prior to the merger is 8–10 m s^{-1} for both V_1 and V_2 due to the opposite wind directions (i.e., east-northeasterly versus west-southwesterly) between 200 and 900 hPa, but it drops to 2–3 m s^{-1} near 18/12–36 with maximum surface winds exceeding 20 m s^{-1} (see Figs. 6b, 6c, and 7). The local VWS within the ITCZ in which V_2 is embedded is much smaller than the area-averaged shear, as can be seen by nearly upright isotachs in Fig. 5a. This abrupt drop in VWS during the merging period is not an artifact of the area average but a result of the merger. That is, both V_1 and V_2 are relatively shallow systems with more visible cyclonic flows up to 400 hPa and some directional shear above (see Figs. 3a and 6b,c). As soon as the two MCVs merge, the storm is strengthened with a deep vortical column with little directional shear (i.e., nearly all southeasterly in the vertical), thereby decreasing VWS significantly (see Figs. 3b and 6b,c). The decreased VWS in Eugene's immediate environment in turn allows the storm to keep deepening for 30–36 h, albeit at a relatively slow rate of 0.3 hPa h^{-1}. Subsequently, the storm begins to weaken, which coincides well with a steady increase in VWS up to 18 m s^{-1} as it moves northwestward away from the moisture supply of the ITCZ.

Figure 8 compares the model-simulated 6-h accumulated rainfall at 12-h intervals during the genesis and deepening stages of Eugene (i.e., 1200 UTC 17 July–0600 UTC 20 July) to the corresponding TRMM satellite product at 0.25° resolution. It is evident that, although the WRF model could not reproduce all the rainfall details, it simulates reasonably well the general magnitude and structures of the observed rainfall. They include the ITCZ-related rainfall belt to the south (Figs. 8a–c), its subsequent northward rollup to form a "comma shaped" rainfall pattern as a closed surface cyclone develops (Figs. 8c–e), the more organized and intense rainfall over the "comma head" region with less rainfall distributed along the "comma tail" (Figs. 8d–f), and the suppressed deep convection over the coastal regions at the later stages (Figs. 8c–f). Note that the northward rollup on the eastern end of the ITCZ is similar to that described by NS97 and WM06. The simulated 6-h maximum rainfall rate exceeds 90 mm, comparable to that observed. Of importance is that both the simulation and TRMM observations show (i) several localized rainfall centers around the surface cyclone, with much greater magnitudes than those in the ITCZ, and (ii) significant rainfall asymmetries with little rainfall occurring to the north of the surface cyclone. As will be shown in the next section, the more localized rainfall centers tend to occur on the downshear left (Frank and Ritchie 2001; Black et al. 2002; Zhang and Kieu 2006). Moreover, if the localized rainfall centers associated with the surface cyclone are traced in time (e.g., Figs. 8a–c), one can see that major convective cells are initiated to the south and then move cyclonically to the west and east of the surface cyclone, though with reduced magnitudes. More intense rainfall occurs when two convective complexes merge (Figs. 8a–c), which is consistent with the merger of the two MCVs mentioned earlier.

While the WRF model reproduces many rainfall features of Eugene, there are significant errors in the position of local rainfall centers (and timing) associated with the comma head due to the westward bias of the simulated track (Fig. 7). These errors are more pronounced during the weakening stage, so the simulated and observed rainfall fields are not compared after the 72-h integration. Despite these errors, the general agreements of tracks, intensity, and rainfall patterns between the simulation and observations indicate that the model reproduces the basic sequence of many processes involved in the genesis and development of Eugene. Thus, the model-simulated high-resolution hourly output data are used in the next sections to examine

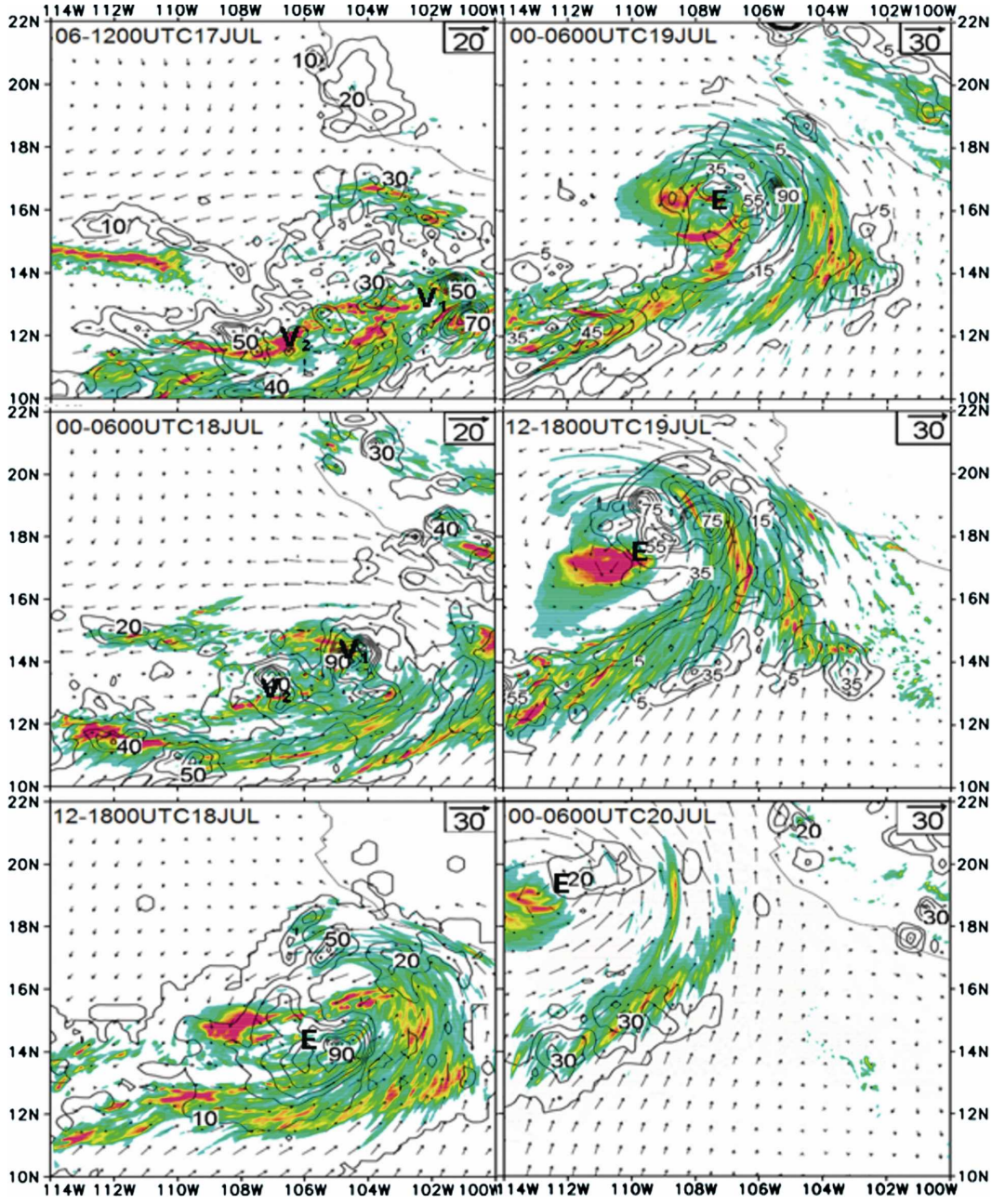

FIG. 8. Comparison of the 6-h accumulated rainfall (mm) valid at the (a) 17/06–06, (b) 18/00–24, (c) 18/12–36, (d) 19/00–48, (e) 19/12–60, and (f) 20/00–72 simulations over a subdomain of C to the corresponding 6-h TRMM satellite-estimated (contoured) rainfall. The simulated surface flow vectors are also provided.

some nonobservable features as well as the effects of VWS on the rainfall distribution during the life cycle of Eugene.

5. Vortex–vortex interaction and their merger

After showing the relationship between Eugene's genesis and the merger of the two MCVs, as also seen in previous studies (e.g., RH97; Simpson et al. 1997), a natural question one may ask is: How critical is the merger to the TCG? Thus, we are motivated to perform numerical sensitivity experiments with perturbed initial conditions and different physics schemes to search for different model solutions of TCG. We find that, in spite of the presence of the two MCVs in all model initial

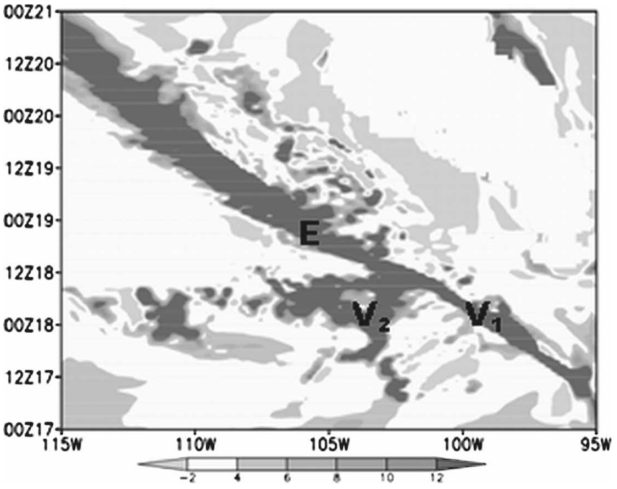

FIG. 9. As in Fig. 1a but for the model simulation during the period from 0000 UTC 17 to 0000 UTC 21 Jul 2005 (i.e., 17/00–00 to 21/00–96) over the longitudinal span of 115°–95°W. It is meridionally averaged within a 1° zone centered through the MCV V_1 (and later Eugene).

conditions, none of the MCVs can even grow into tropical depression strength by 72 h into the integration (to be shown in a forthcoming paper) when they either fail to merge or merge too late (e.g., up to 48 h into the integration). Therefore, we conclude (i) that the ITCZ provides a favorable environment with dynamical instability, high background vorticity, and humidity, but the merger of the two MCVs is essential for the genesis of Eugene, and (ii) that the internal ITCZ breakdowns, as discussed by NS97, are not sufficient for the genesis of Eugene, even in the presence of latent heat release and the Charney–Stern instability. In fact, despite its smaller size, V_1 plays an important role in determining not only the track (see Figs. 1, 6, and 9) but also the TCG, as will be further shown below.

As the aforementioned coalescence and capture phenomenon has not been documented before, let us examine in three dimensions how the two MCVs interacted and merged to cause the genesis of Eugene so as to compare its pertinent scenarios to the merging MCVs cases reported in previous studies. Figure 9 shows that the simulated MCVs begin spin up at 17/18–18 over the 4-km grid. Moreover, they show reduced widths, especially V_1 after the 1.33-km grid domain is activated at 18/00–24. The two MCVs commence to merge at 18/09–33, about 3–6 h later than the observed (cf. Figs. 9 and 2); the merging processes are, as expected, much better resolved temporally and spatially than the NCEP reanalysis (cf. Figs. 9 and 1). The (north-northeastward) drift of V_2 associated with the rollup of the ITCZ compared to the (northwestward) propagation of V_1 and their relative sizes prior to the merger are also evident in Fig. 9—to a certain degree consistent with the satellite imagery and the associated rainfall field (Figs. 2 and 8). Note the increased width at the time of merging (i.e., 18/12–36) but its reduced width immediately afterward, due mainly to the longitudinal averaging of the merging MCVs as V_1 moves cyclonically from the east to north side of V_2 (see Fig. 6) by 18/18–42. As will be seen, the complete merging does not occur until 19/00–48, taking a total of 15 h (i.e., from 18/09–33 to 19/00–48). Note also that V_2 is not as well structured as V_1 because of different locations of peak relative vorticity in the vertical, that is, 800 hPa for V_1 and 700 hPa for V_2 (not shown).

Figure 10 shows the simulated flow and reflectivity fields at the surface and 200 hPa and PV at 500 hPa before, during, and after the merging stage; Fig. 11 shows the corresponding vertical cross sections of the tangential flows and PV through the MCVs/storm centers. The WRF simulates an intense, but small-sized, V_1 with minimum surface pressure 1004 hPa and a RMW ~100 km and a relatively weak and broad scaled V_2 with a closed isobar of 1007 hPa and a RMW of 200 km prior to the merger (Fig. 11a). Note that the size of V_1 has shrunk by half, as it intensifies, from that at the model initial time (cf. Figs. 1–3 and 10). These features conform more or less to those seen from satellite imageries (see Fig. 2). Organized deep convection associated with the two MCVs produces significant concentration of PV in banded structures in the layer 600–400 hPa where the latent heating and upward motion peak. Of interest is the fact that despite the pronounced PV, one can only see the two closed cyclonic circulations of the MCVs above 700 hPa with little closed rotation below (Fig. 11a,b). This is because the penetration depth (Δz) is still shallow for dynamically small vortices ($L \ll L_R$, where L_R is the radius of Rossby deformation) and small magnitudes of PV or the absolute vorticity (ζ_a) anomalies; that is,

$$\Delta z = (f\zeta_a)^{1/2} L/N, \tag{1}$$

where f is the Coriolis parameter and N is the static stability (see Hoskins et al. 1985).

At lower levels, the two MCVs appear to compete with each other for convective available potential energy (CAPE) for convective development in their southern semicircles when they are near proximity (e.g., 450 km). More higher θ_e air in the ITCZ is converged into the convective regions of V_1 (Fig. 10), generating the most intense convection in its southeastern quadrant, as can be seen at 200 hPa. The intense convective cells coincide with the strong signals seen in

satellite imagery at 0300 and 0600 UTC 18 July (cf. Figs. 2 and 10). In this regard, V_1 intensifies at the expense of V_2, and the latter has soon become a wake MCV of the former. Note that deep convection always occurs some distance away from the surface cyclone center, suggesting that convectively generated compensating subsidence warming accounts for the formation of a rain-free, "eyelike" region at the storm center. Higher up, both MCVs generate strong divergent winds aloft that are superimposed on the upper-level easterly flow.

At 18/12–36, V_2 has almost lost its identity in reflectivity and surface circulations in the wake of a to-be-formed TD, as the low to midlevel PV increases in magnitude and volume and the distance between the two MCVs shortens by half (Fig. 10). Clearly, the increased surface winds (up to 22 m s^{-1}, see Fig. 7) help initiate the wind-induced surface heat exchange (WISHE) process leading to the subsequent TCG (Rotunno and Emanuel 1987). Of importance is the fact that, despite its weakness, the general midlevel flow pattern is still dominated by the V_2-related circulation owing to the larger volume it occupies. As a result, the V_2-related southerly flow tends to offset the northerly flow associated with V_1 in the vertical before their complete merger (see Fig. 11).

By 18/18–42, a well-organized surface cyclone has developed, and the two MCVs would be considered as having merged if only the surface circulations are concerned. However, we can still see an elongated circulation with identifiable V_2 remnant flow and PV at the midlevel. Evidently, despite its stronger intensity, it is V_1 that has "impinged" on the V_2 circulation and is later absorbed by V_2 because of the slower pace and larger volume of V_2. Nevertheless, the volume of the merged circulation has shrunk substantially during the previous 12-h period, with the distribution of concentrated PV stripes within it, leading to the pronounced deepening of the storm at the broad scale (Fig. 10).

Although the two MCVs are completely merged at 19/00–48, the merged circulations are better defined 6 h later, so the results at 19/06–54 are shown here as well. At this latter time, the merger is characterized by the development of deep convection in all quadrants—though still as a comma head of the ITCZ rollup and a deep column of PV near the vortex center with well-defined tangential flows around it and anticyclonic outflows aloft. It has a RMW of ~200 km, which is similar to that of V_2 (Fig. 11). Note that a spiral rainband in the southeastern quadrant produces intense anticyclonic outflows aloft that appear to block the influence of the upper-level easterly flow, thus protecting the vortex core temporally from VWS or dry-air intrusion (Figs. 10 and 11). This seems to be consistent with the development of deep convection in all quadrants when the MCVs are merged at 19/06–54, in contrast to the wavenumber-1 structures seen at the other hours (see Fig. 12). Note also that the storm has begun to experience the influence of approaching outflows associated with Hurricane Emily (2005), as indicated by limited eastward expansion of its anticyclonic flows aloft along the east boundary (Fig. 10).

It should be noted that the tangential flows peak at the midlevel prior to the merger (Fig. 11a). During the merging period, the tangential flows increase much more rapidly in the lower troposphere than at the midlevel (cf. Figs. 11a–d), in pace with the deepening of the storm; the PV (or relative vorticity) in the "eye" behaves similarly. This scenario differs from the simple "downward growth of the midlevel relative vorticity" proposed by RH97 in which merging MCVs occur within a low-level, larger-scale cyclonic system. As will be shown in Part II, the rapid increase in the low to midlevel PV results from the merging of many small vortices with high PV in the lower half of the troposphere, and the storm-scale absolute vorticity tends to grow from the bottom upward through stretching.

6. Effects of vertical wind shear

Previous studies have shown the effects of VWS on the development of wavenumber-1 precipitation structures of hurricanes in which isentropic surfaces across the eye are markedly deformed (Frank and Ritchie 2001; Black et al. 2002; Zhang and Kieu 2006). It is unclear to what extent such a conceptual model could be applied to a weak tropical storm, like Eugene, in which isentropic surfaces are weakly deformed. For this purpose, Fig. 12 shows the evolution of the simulated radar reflectivity, horizontal flow, and area-averaged hodographs at 12-h intervals from the 36–96-h simulations. One can see the development of more (small scale) intense convective cells during the genesis stage, as indicated by the radar reflectivity >50 dBZ. This is particularly true in the southern semicircle at 19/12–60 when the storm reaches peak intensity. As can be seen from Figs. 12–14, this active convection region around the rain-free eye is similar in many characters to the eyewall associated with a hurricane. (Of course, the simulated eye is not free of clouds because they have little contribution to radar reflectivity.) After the storm reaches peak intensity, weaker and larger-sized convective cells develop in the "eyewall" with most precipitation being stratiform during the decaying stage (e.g., at 21/00–96).

On the other hand, the large-scale mean flow has been substantially disturbed, including the midlevel jet,

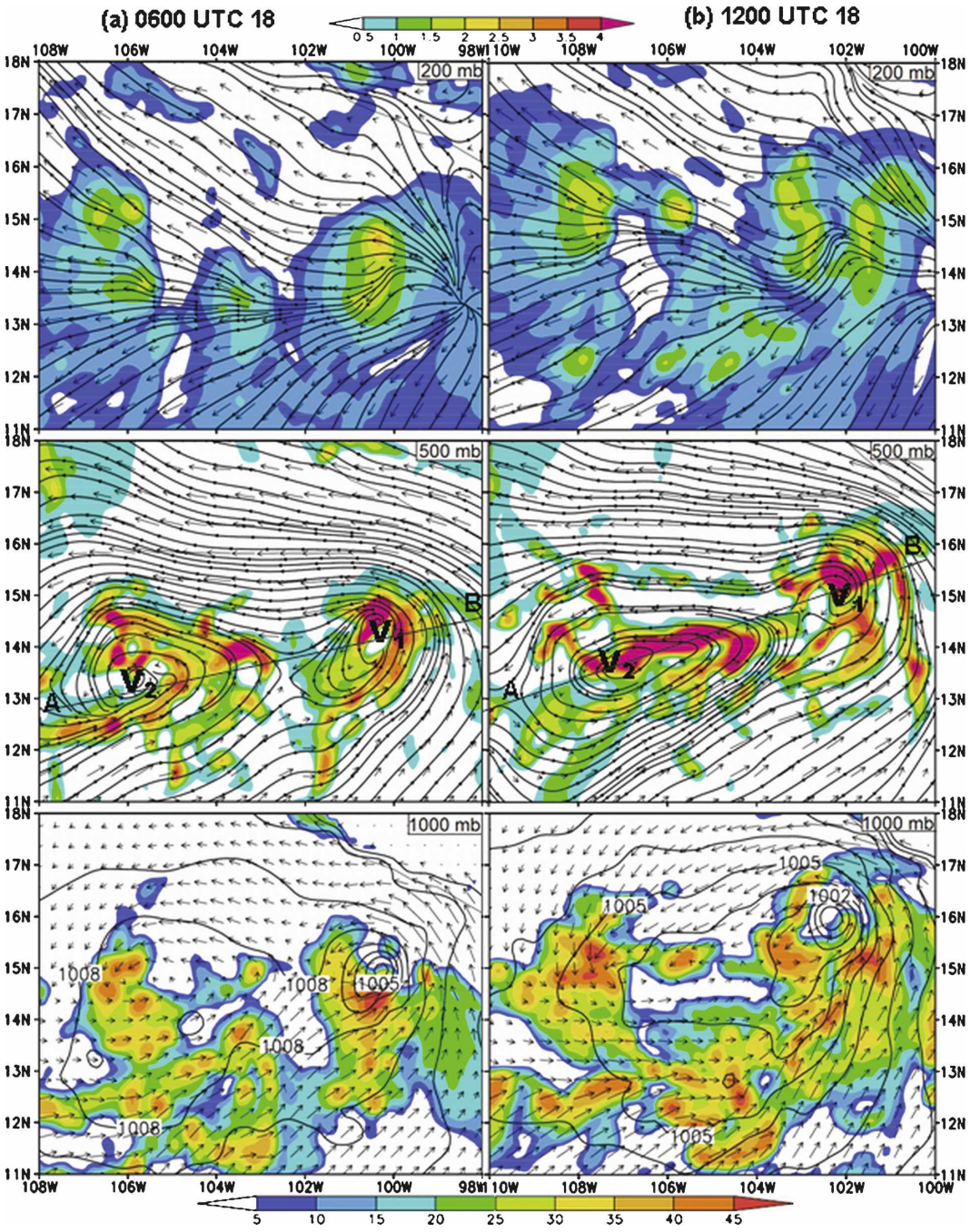

FIG. 10. Horizontal distribution of the (bottom) sea level pressure (at intervals of 1 hPa) and flow vectors, (middle) flow vectors and streamlines at 500 hPa, and (top) flow vectors and streamlines at 200 hPa over a subdomain of C at (a) 18/06–30, (b) 18/12–36, (c) 18/18–42, and (d) 19/06–54.

due to the upstream influence of Emily and the development of Eugene (cf. Figs. 5a and 12). For example, the northwestward rollup of the ITCZ by Eugene brings in tropical large-scale southwesterly flow and forces the midlevel easterly flow to go northwestward (e.g., see Fig. 10), thereby giving rise to northwestward wind shifts in the mean flows at 700 and 500 hPa between 19/12–60 and 20/12–84. As a result, the mean VWS shifts from easterly at 8 m s^{-1} prior to the merger to northeasterly at 12–14 m s^{-1} near the end of the 4-day integration.

Given the VWS in selected layers, it is important to

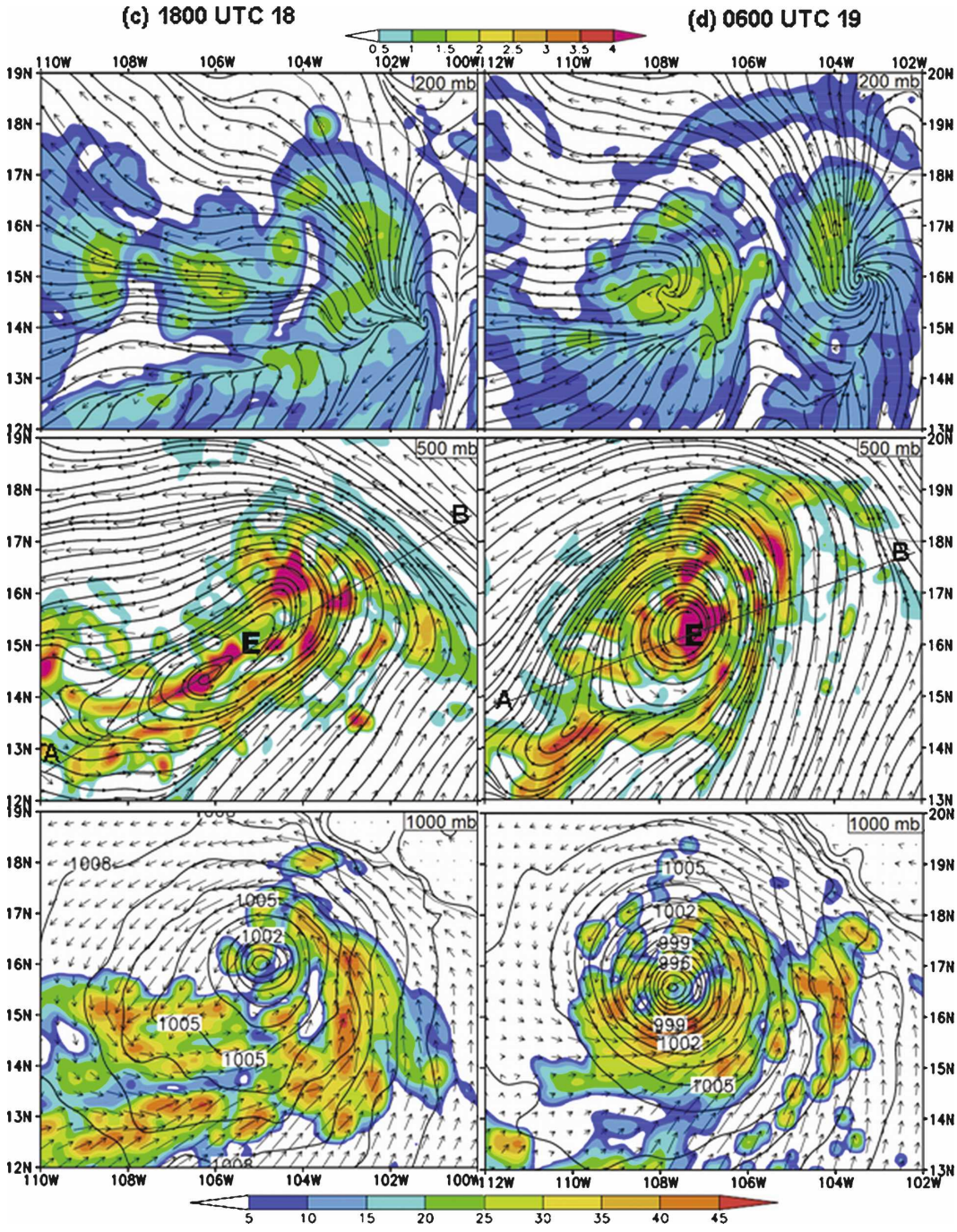

FIG. 10. (*Continued*) Shadings in the top and bottom panels are for the simulated radar reflectivity, at intervals of 5 dB*Z*, and in the middle panels are for PV, at intervals of 0.5 PVU. Line AB shows vertical cross sections used in Fig. 11. All flows are system relative.

note that more intense precipitation in the inner-core region occurs more or less in the southwestern quadrant or on the downshear-left side of the storm except at the final dissipated stage (i.e., at 21/00–96), particularly when the 500–900-hPa layer VWS, which better represents the effects of the midlevel jet, is considered. The development of a warm-core structure, as shown in Figs. 13 and 14, supports the downshear-left distribution of precipitation at this early stage of a TS. Such a downshear-left asymmetry is not applicable at 21/00–96 with respect to the deep-layer VWS but is still valid when the 700–900-hPa VWS is considered. This consid-

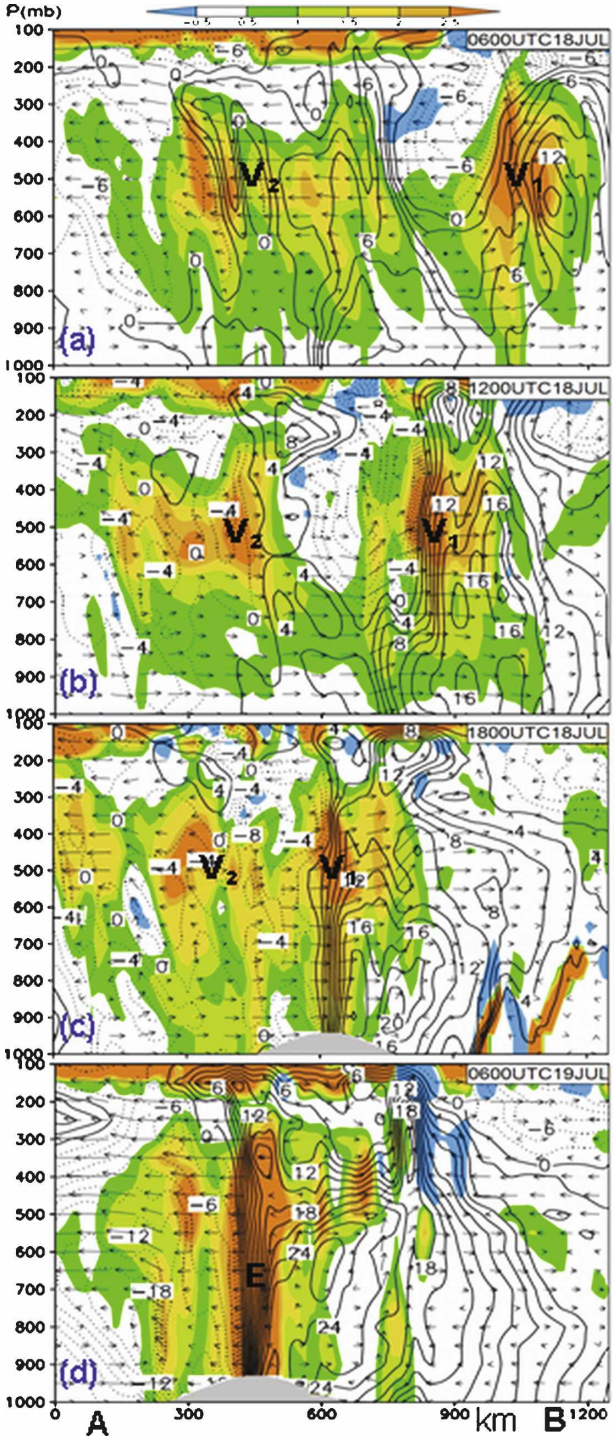

FIG. 11. As in Fig. 10 but for the three-slice-averaged (i.e., 4 km) vertical cross sections of the normal component of horizontal winds (at 2 m s^{-1} intervals) and PV (shaded at intervals of 0.5 PVU), superimposed by the system-relative in-plane flow vectors along the centers of V_1 and V_2 (see Fig. 10 for their locations). Note that the vertical wind component has been amplified by a factor of 10.

eration is justifiable in view of the fact that Eugene has become a weak and shallow MCV at this time. Moreover, the weak convective rainfall on the downshear-right side still occurs in the favorable semicircle of uplifting, according to Zhang and Kieu (2006).

Note that the VWS vectors rotate with height at 19/12–60 and 20/00–72, which appears to complicate the simple relationship between the mean VWS and its induced vertical motion. According to Zhang and Kieu, the VWS-induced vertical motion at any vertical layer results from the summed vertical motion induced by the VWS from all vertical layers, although it is more dominated by the VWS at the same layer. Thus, the vertical rotation of VWS may account to a certain extent for the generation of downshear-right precipitation. Of course, convective developments in the outer region (i.e., about 200 km outward from the center) are more related to the rollup of the ITCZ feeding CAPE into the storm, but they weaken while propagating cyclonically to the northern semicircle where the atmospheric conditions are less favorable, including the presence of strong VWS.

Figure 13 shows the three-dimensional distribution of a constant θ_e surface (i.e., 352 K), denoting roughly the eyewall at two different stages, so as to gain insight into the effects of VWS on the vertical structures of the storm. Evidently, Eugene exhibits little vertical tilt at the most intense stage during which VWS is less than 5 m s^{-1} (cf. Figs. 7b and 13a). In addition, we can see pronounced convectively generated warming and moistening (i.e., high-θ_e air) in the inner-core region in the upper troposphere, as also shown in vertical θ_e cross sections in Fig. 14. By comparison, the storm begins to tilt west-to-southwestward as VWS increases. Meanwhile, the volume of high-θ_e air in the PBL shrinks, feeding less CAPE to the eyewall for convective development. As a result, the volume of high-θ_e air in the upper outflow layer decreases, which coincides with less convective development in the eyewall and subsequent weakening of the storm (cf. Figs. 7, 12, and 13b).

Figure 14 shows the effects of VWS on the initiation of moist downdrafts, more significantly in the midlevel minimum-θ_e layer (i.e., near 700 hPa herein), on the upshear side of the storm, which coincides with downward motion as induced by vertical shear (see Zhang and Kieu 2006). As in Fig. 13, one can see the high-θ_e air in the inner-core region, but the highest θ_e values (i.e., $\theta_e > 354$ K) appearing in the eyewall result from the convective transport of high-θ_e air from the PBL in "vortical hot towers" (Fig. 14a). This is in contrast to the low-θ_e intrusion (i.e., $\theta_e < 342$ K) from the vast source region to the west of the storm. Of relevance here is the development of wide downdraft bands out-

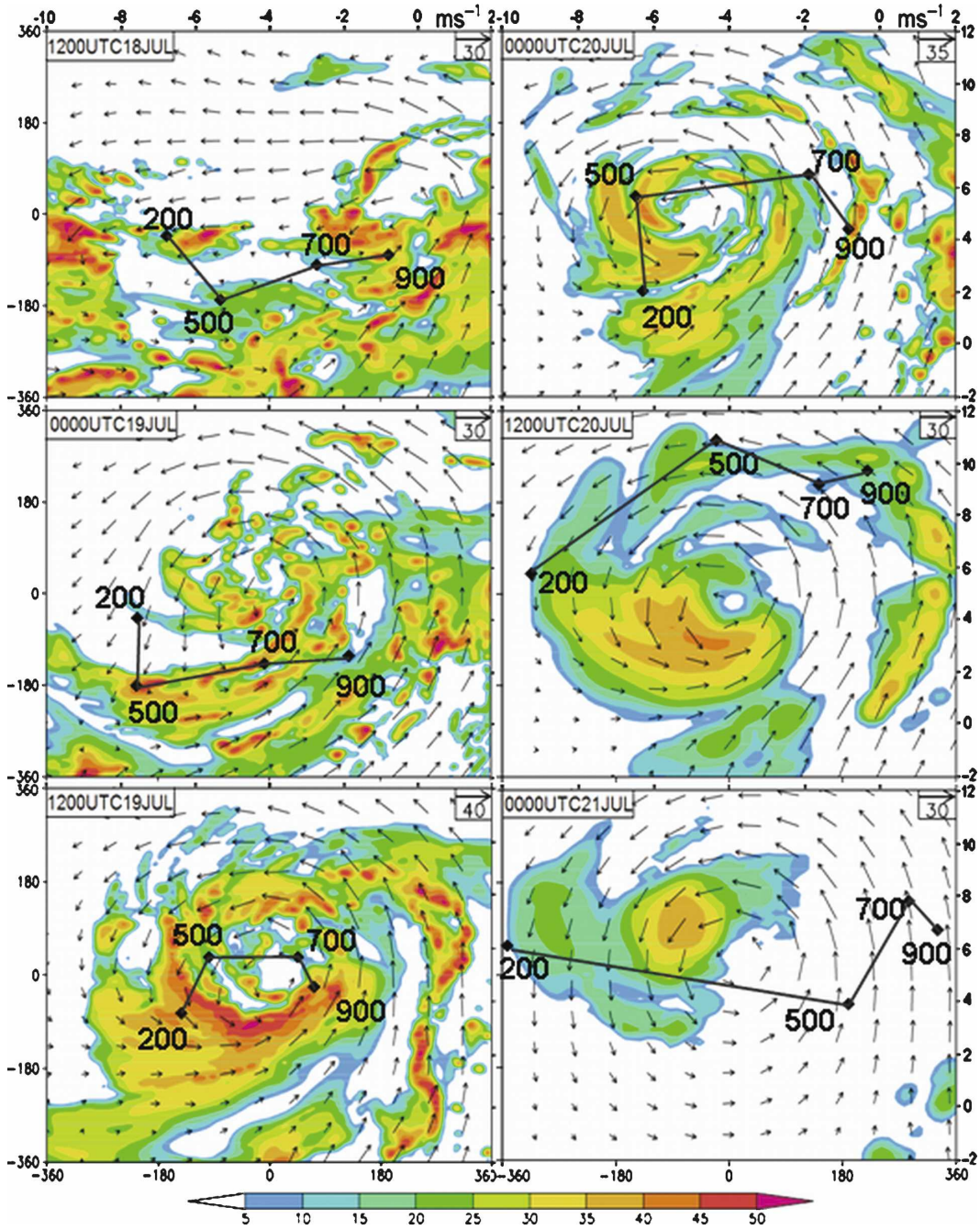

FIG. 12. Horizontal distribution of the radar reflectivity (shaded at 5-dBZ intervals) and flow vectors at 850 hPa at 18/12–36, 19/00–48, 19/12–60, 20/00–72, 20/12–84, and 21/00–96 over a subdomain of C. Hodographs with vertical shear vectors (solid) between 900 and 200 hPa, obtained by averaging them over an area of 800 km × 800 km at the storm center, are sketched with the speed scale given on the top and right frames.

side the eyewall, more significantly on the upshear side with respect to the shear vector in the 700–900-hPa layer (Fig. 14a). Similar features have also been observed in the upper troposphere in the simulation of Hurricane Bonnie (1998) owing to the presence of an intense deep-layer (200–900 hPa) unidirectional VWS of 18 m s^{-1} (see Figs. 8 and 16 in Zhu et al. 2004).

Vertical θ_e cross sections show that the downdraft bands are generated by convergence of the midlevel lower-θ_e air toward the eyewall clouds, that is, the dry

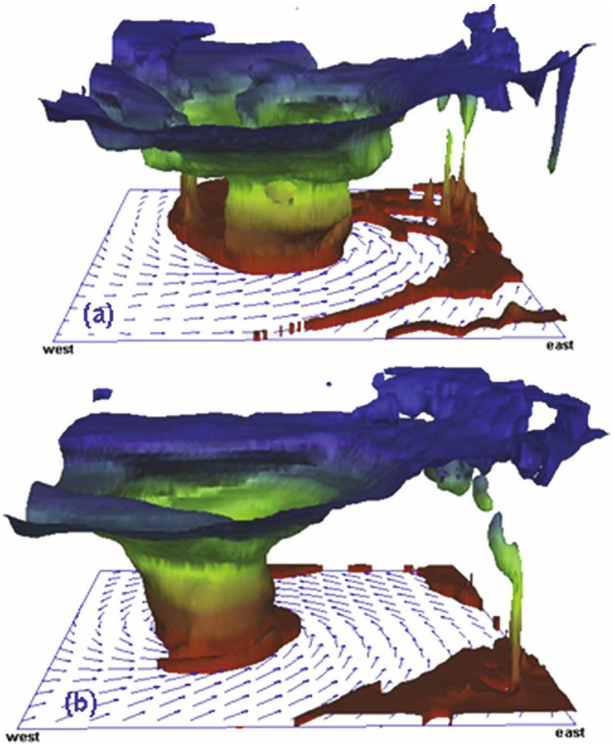

FIG. 13. Three-dimensional view (800 km × 800 km × 12 km) of the θ_e = 352 K isosurface superimposed by the storm-relative surface flow vectors from a subdomain of C at (a) 19/18–66 and (b) 20/06–78.

intrusion (Figs. 14b,c). These downdrafts do not seem to be (dry) isentropically, induced by VWS as described by Raymond and Jiang (1990) and Fritsch et al. (1994), but are evaporatively driven, because (positive) potential temperature perturbations (θ') only occur in the eye close to active eyewall convection (see Figs. 14b,c). The penetrative moist downdraft air carrying the midlevel lower θ_e values would be advected cyclonically in the PBL such that deep convection will be suppressed downstream in the eyewall, likely enhancing the precipitation asymmetry in the eyewall and weakening the storm. Obviously, the midlevel convergence of low-θ_e air is unfavorable for TCG, in contrast to the typical low-level convergence of higher-θ_e air. Furthermore, cold moist downdrafts, occurring side by side with the eyewall updrafts, tend to strengthen the θ_e (and temperature) gradients across the eyewall (cf. Figs. 14b,c). Thus, the upshear generation of moist downdrafts through dry intrusion may be considered as the thermodynamical impact of VWS on TCG as well as on MCSs and deep convection, in contrast to the VWS-induced dynamical (isentropic) lifting in MCSs and TCs (Raymond and Jiang 1990; Zhang and Kieu 2006).

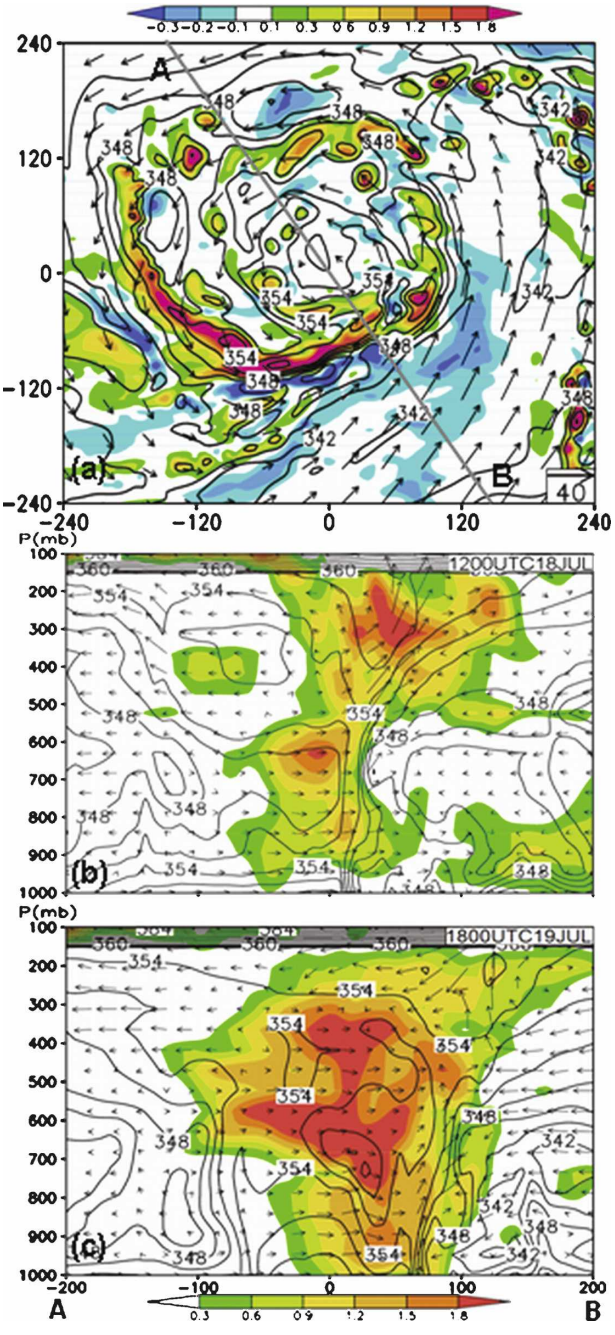

FIG. 14. (a) Horizontal distribution of θ_e (at intervals of 2 K), in-plane flow vectors, and vertical motion (shaded at intervals 0.1 m s^{-1} for descending and 0.3 m s^{-1} for ascending motion) at 700 hPa at 19/12–60. (b), (c) Vertical cross section of θ_e (at intervals of 2 K), storm-relative in-plane flow vectors, and deviation potential temperature (θ', shaded) along the 700–900 hPa VWS vector through the storm center at (b) 19/12–60 and (c) 19/18–66. Line AB in (a) shows the three-slice-averaged (i.e., 4 km) vertical cross sections used in (b) and (c).

Note the bifurcation of vertical circulation associated with the midlevel convergence of lower-θ_e air in the environment: one branch entering the eyewall updrafts above the minimum-θ_e layer and the other branch forming moist downdrafts below. The upper-level lower-θ_e air intrusions can be cyclonically advected into the storm owing to the presence of less inertial stability aloft. This will cause weakening of the convective updrafts in the eyewall, and in some cases induce moist downdrafts in the upper levels as shown by Zhu et al. (2004). Note also the strong asymmetries in the subsidence warming and secondary circulations in the vicinity of active convection, which are different from those seen in hurricanes (e.g., Liu et al. 1997; Zhu et al. 2004; Zhang and Kieu 2006). The pronounced convergent flows in the lower-level inner-core region should not be considered as radial flows but, rather, as being caused mostly by the vertical tilt and asymmetries of the eyewall.

7. Summary and conclusions

In this study, TCG from merging MCVs associated with the ITCZ breakdowns is examined through a case study of the processes leading to the genesis of TS Eugene (2005) over the eastern Pacific from its pregenesis to dissipation stages. This is achieved by using the NCEP reanalysis, satellite data, and the best-track analysis, and by performing 4-day (0000 UTC 17–0000 UTC 21 July 2005) two-way interactive, movable, multinested, cloud-resolving simulations using the WRF model with the finest grid size of 1.33 km. The dynamical and thermodynamic effects of VWS associated with a midlevel easterly jet on the genesis and dissipation, as well as the three-dimensional structures of the storm, are also explored.

Observational analyses reveal that Eugene grew out of two merging midlevel MCVs: one (V_1) initiated before 0000 UTC 11 July on the eastern end of the ITCZ breakdown and the second (V_2) spawned 2 days later from the ITCZ at a distance of 1000 km from V_1; both had initial size of about 400 km in diameter. The earlier ITCZ breakdown appeared to be associated with interrupted moisture convergence by trade winds over the Central American continent, whereas the growth of V_2 resulted in another ITCZ breakdown and its subsequent poleward rollup due to the presence of the Charney–Stern instability. The two MCVs moved at similar speeds northwestward, while keeping a distance of 900–1100 km in between, offshore along the Mexican coast during the first 3 days after the formation of V_2. Later, however, V_2 began to move slowly north-northeastward in association with the poleward rollup of the ITCZ, while V_1 moved at nearly the same velocity as before. It was the track change of V_2 that allowed the two MCVs to merge 2–3 days afterward, leading to the genesis of Eugene.

Although the WRF model is initialized at 0000 UTC 17 July with the NCEP reanalysis without any bogus data, it reproduces the different movements of the two midlevel MCVs with few surface signals, the intensification and size shrinkage of V_1 at the later stages, their merging interactions at nearly the right timing and location at 39 h into the integration, and the subsequent track and intensity of the merger in association with the poleward rollup of the ITCZ. Model results show that the two MCVs interact and merge into a coalescence and capture mode; namely, V_1 impinges on the V_2 circulation and is then captured by V_2. Merging of the two relatively shallow systems reduces rainfall asymmetries with deep convection in all quadrants, likely accounting for the pronounced reduction of larger-scale VWS in a deep layer and allowing the merger to deepen quickly to TS (Eugene) intensity. As the two MCVs merge, the low to mid level PV and tangential flows increase substantially; the latter occurs more rapidly in the lower troposphere, helping initiate the WISHE process leading to the genesis of Eugene. Subsequently, Eugene moves northwestward, retaining the characters of both MCVs. The merging scenarios appear to differ from those presented in RH97 in which MCVs merged within a larger-scale cyclonic system. It is found from sensitivity simulations that, in spite of the presence of the Charney–Stern instability in the vicinity of the ITCZ, none of the MCVs could grow into tropical depression strength when they either fail to merge or merge too late.

It is shown that the simulated tropical storm exhibits many features similar to a hurricane, such as the warm-cored "eye" and the rotating "eyewall" as seen from the radar reflectivity, strong thermal gradients across the eyewall, RMW, and spiral rainbands. It is found that strong VWS associated with the midlevel jet could also force the storm to tilt downshear and produce typical wavenumber-1 rainfall structures during the genesis stage, which are similar to those found in hurricanes. In addition, VWS has a thermodynamical impact on the upshear generation of moist downdrafts in the vicinity of the eyewall as a result of dry air intrusion, particularly in the minimum-θ_e layer. Based on the aforementioned results, we may conclude that the ITCZ breakdown provides a favorable environment with dynamical instability, high humidity, and background vorticity, but the merger of the two MCVs is critical for the genesis of Eugene. The storm decays as it moves northwestward, farther away from the ITCZ into an environment with

increasing VWS, dry intrusion, colder SST, and dynamical stability. Because the ITCZ breakdown occurs frequently during the warm season, the above results appear to have some important implications for the high density of TCG events over the eastern Pacific.

In Part II of this series of papers, we will examine in more detail the merging kinematics and dynamics using high-resolution simulation data, focusing especially on how the low- to midlevel PV and cyclonic rotation increase during the merging period, so as to gain better insight into the roles of the vortex merger in the genesis of Eugene.

Acknowledgments. We thank two anonymous reviewers for their constructive comments that helped significantly improve the quality of the manuscript. This work was supported by NASA Grant NNG05GR32G and NSF Grant ATM0758609. The computations were performed at the Department of Atmospheric and Oceanic Science, University of Maryland.

REFERENCES

Agee, E. M., 1972: Note on ITCZ wave disturbances and formation of Tropical Storm Anna. *Mon. Wea. Rev.,* **100,** 733–737.

Avila, L. A., and R. J. Pasch, 1992: Atlantic tropical systems of 1991. *Mon. Wea. Rev.,* **120,** 2688–2696.

Bister, M., and K. A. Emanuel, 1997: The genesis of Hurricane Guillermo: TEXMEX analyses and a modeling study. *Mon. Wea. Rev.,* **125,** 2662–2682.

Black, M. L., J. F. Gamache, F. D. Marks, C. E. Samsury, and H. E. Willoughby, 2002: Eastern Pacific Hurricanes Jimena of 1991 and Olivia of 1994: The effect of vertical shear on structure and intensity. *Mon. Wea. Rev.,* **130,** 2291–2312.

Bosart, L. F., and F. Sanders, 1981: The Johnstown flood of July 1977: A long-lived convective storm. *J. Atmos. Sci.,* **38,** 1616–1642.

Challa, M., and R. L. Pfeffer, 1990: Formation of Atlantic hurricanes from cloud clusters and depressions. *J. Atmos. Sci.,* **47,** 909–927.

Charney, J. G., and M. Stern, 1962: On the stability of internal baroclinic jets in a rotating atmosphere. *J. Atmos. Sci.,* **19,** 159–172.

DeMaria, M., 1996: The effect of vertical shear on tropical cyclone intensity change. *J. Atmos. Sci.,* **53,** 2076–2087.

Dickinson, M., and J. Molinari, 2002: Mixed Rossby–gravity waves and western Pacific tropical cyclogenesis. Part I: Synoptic evolution. *J. Atmos. Sci.,* **59,** 2183–2196.

Emanuel, K. A., 2000: A statistical analysis of tropical cyclone intensity. *Mon. Wea. Rev.,* **128,** 1139–1152.

Frank, W. M., and E. A. Ritchie, 2001: Effects of vertical wind shear on the intensity and structure of numerically simulated hurricanes. *Mon. Wea. Rev.,* **129,** 2249–2269.

Fritsch, J. M., J. D. Murphy, and J. S. Kain, 1994: Warm core vortex amplification over land. *J. Atmos. Sci.,* **51,** 1780–1807.

Gray, W. M., 1968: Global view of the origin of tropical disturbances and storms. *Mon. Wea. Rev.,* **96,** 669–700.

Hack, J. J., W. H. Schubert, D. E. Stevens, and H.-C. Kuo, 1989: Response of the Hadley circulation to convective forcing in the ITCZ. *J. Atmos. Sci.,* **46,** 2957–2973.

Halverson, J., and Coauthors, 2007: NASA's Tropical Cloud Systems and Processes Experiment. *Bull. Amer. Meteor. Soc.,* **88,** 867–882.

Harr, P. A., and R. L. Elsberry, 1996: Structure of a mesoscale convective system embedded in Typhoon Robyn during TCM-93. *Mon. Wea. Rev.,* **124,** 634–652.

——, M. S. Kalafsky, and R. L. Elsberry, 1996: Environmental conditions prior to formation of a midget tropical cyclone during TCM-93. *Mon. Wea. Rev.,* **124,** 1693–1710.

Hoskins, B. J., M. E. McIntyre, and A. W. Robertson, 1985: On the use and significance of isentropic potential vorticity maps. *Quart. J. Roy. Meteor. Soc.,* **111,** 877–946.

Jones, S. C., 1995: The evolution of vortices in vertical shear. I: Initially barotropic vortices. *Quart. J. Roy. Meteor. Soc.,* **121,** 821–851.

Kain, J. S., and J. M. Fritsch, 1990: A one-dimensional entraining/detraining plume model and its application in convective parameterization. *J. Atmos. Sci.,* **47,** 2784–2802.

Lander, M., and G. J. Holland, 1993: On the interaction of tropical-cyclone-scale vortices. I. Observations. *Quart. J. Roy. Meteor. Soc.,* **119,** 1347–1361.

Li, X., and B. Wang, 1994: Barotropic dynamics of the beta gyres and beta drift. *J. Atmos. Sci.,* **51,** 746–756.

Lin, Y.-L., R. D. Farley, and H. D. Orville, 1983: Bulk parameterization of the snow field in a cloud model. *J. Appl. Meteor.,* **22,** 1065–1092.

Liu, Y., D.-L. Zhang, and M. K. Yau, 1997: A multiscale numerical study of Hurricane Andrew (1992). Part I: Explicit simulation and verification. *Mon. Wea. Rev.,* **125,** 3073–3093.

McBride, J. L., and R. Zehr, 1981: Observational analysis of tropical cyclone formation. Part II: Comparison of non-developing versus developing systems. *J. Atmos. Sci.,* **38,** 1132–1151.

Mlawer, E. J., S. J. Taubman, P. D. Brown, M. J. Iacono, and S. A. Clough, 1997: Radiative transfer for inhomogeneous atmospheres: RRTM, a validated correlated-*k* model for the longwave. *J. Geophys. Res.,* **102,** 16 663–16 682.

Molinari, J., D. Knight, M. Dickinson, D. Vollaro, and S. Skubis, 1997: Potential vorticity, easterly waves, and eastern Pacific tropical cyclogenesis. *Mon. Wea. Rev.,* **125,** 2699–2708.

——, D. Vollaro, S. Skubis, and M. Dickinson, 2000: Origins and mechanisms of Eastern Pacific tropical cyclogenesis: A case study. *Mon. Wea. Rev.,* **128,** 125–139.

Nieto Ferreira, R., and W. H. Schubert, 1997: Barotropic aspects of ITCZ breakdown. *J. Atmos. Sci.,* **54,** 261–285.

Raymond, D. J., and H. A. Jiang, 1990: A theory for long-lived mesoscale convective systems. *J. Atmos. Sci.,* **47,** 3067–3077.

Reasor, P. D., M. T. Montgomery, and L. F. Bosart, 2005: Mesoscale observations of the genesis of Hurricane Dolly (1996). *J. Atmos. Sci.,* **62,** 3151–3171.

Ritchie, E. A., and G. J. Holland, 1997: Scale interactions during the formation of Typhoon Irving. *Mon. Wea. Rev.,* **125,** 1377–1396.

Rotunno, R., and K. A. Emanuel, 1987: An air–sea interaction theory for tropical cyclones. Part II: Evolutionary study using a nonhydrostatic axisymmetric numerical model. *J. Atmos. Sci.,* **44,** 542–561.

Simpson, J., E. Ritchie, G. J. Holland, J. Halverson, and S. Stewart, 1997: Mesoscale interactions in tropical cyclone genesis. *Mon. Wea. Rev.,* **125,** 2643–2661.

Skamarock, W. C., J. B. Klemp, J. Dudhia, D. O. Gill, D. M. Barker, W. Wang, and J. G. Powers, 2005: A description of

the Advanced Research WRF, version 2. NCAR Tech. Note NCAR/TN-468+STR, 88 pp.

Wang, C.-C., and G. Magnusdottir, 2006: The ITCZ in the central and eastern Pacific on synoptic time scales. *Mon. Wea. Rev.,* **134,** 1405–1421.

Wang, Y., and G. J. Holland, 1996: Tropical cyclone motion and evolution in vertical shear. *J. Atmos. Sci.,* **53,** 3313–3332.

Wu, C.-C., and K. A. Emanuel, 1993: Interaction of a baroclinic vortex with background shear: Application to hurricane movement. *J. Atmos. Sci.,* **50,** 62–76.

Zehnder, J. A., D. M. Powell, and D. L. Ropp, 1999: The interaction of easterly waves, orography, and the intertropical convergence zone in the genesis of eastern Pacific tropical cyclones. *Mon. Wea. Rev.,* **127,** 1566–1585.

Zhang, D.-L., and N. Bao, 1996a: Oceanic cyclogenesis as induced by a mesoscale convective system moving offshore. Part I: A 90-h real-data simulation. *Mon. Wea. Rev.,* **124,** 1449–1469.

——, and ——, 1996b: Oceanic cyclogenesis as induced by a mesoscale convective system moving offshore. Part II: Genesis and thermodynamic transformation. *Mon. Wea. Rev.,* **124,** 2206–2226.

——, and C. Q. Kieu, 2006: Potential vorticity diagnosis of a simulated hurricane. Part II: Quasi-balanced contributions to forced secondary circulations. *J. Atmos. Sci.,* **63,** 2898–2914.

Zhu, T., D.-L. Zhang, and F. Weng, 2004: Numerical simulation of Hurricane Bonnie (1998). Part I: Eyewall evolution and intensity changes. *Mon. Wea. Rev.,* **132,** 225–241.